Variational method with staggered fermions

Carleton DeTar and Song-Haeng Lee

Phys. Rev. D **91**, 034504 — Published 11 February 2015

DOI: 10.1103/PhysRevD.91.034504

Variational method with staggered fermions

Carleton DeTar and Song-Haeng Lee
Department of Physics and Astronomy,
University of Utah, Salt Lake City, Utah

Abstract

The variational method is used widely for determining the hadronic spectrum for Wilson and improved Wilson fermions. The method has not been applied to staggered fermions because the hadronic correlation functions in that formalism include terms that oscillate with Euclidean time, and they often include states of both parities. We show that with a simple modification, the variational method can also be applied to staggered fermions. In some cases the method also provides a mechanism for separating the commonly paired parity-partner states. We discuss the extension to staggered fermions and illustrate it by applying it to the calculation of the spectrum of charmed-antistrange mesons consisting of a clover charm quark and a staggered strange antiquark.

I. CONVENTIONAL WILSON VARIATIONAL METHOD

We consider the hadronic correlator for propagation from Euclidean time 0 to time t (an integer in lattice units):

$$C_{ij}(t) = \langle 0|\mathcal{O}_i(t)\mathcal{O}_j^\dagger(0)|0\rangle\,, \tag{1.1}$$

generated by a set of hermitian interpolating operators $\mathcal{O}_i(t)$ and propagating according to the QCD hamiltonian H derived from an action with a single time-step transfer matrix $T = \exp(-H)$. We assume the time extent of the lattice is sufficiently large that we may consider propagation only forward in time. Then, eigenstates of the hamiltonian with energy E_n correspond to eigenstates of the transfer matrix T with eigenvalue $\exp(-E_n)$. (We enumerate energies in ascending order.) In terms of these eigenstates, the correlator has a multiexponential eigenenergy representation

$$C_{ij}(t) = \sum_n \langle 0|\mathcal{O}_i(t)|n\rangle e^{-E_n t}\langle n|\mathcal{O}_j^\dagger(0)|0\rangle\,, \tag{1.2}$$

or in matrix form

$$C(t) = ZT^tZ^\dagger\,, \tag{1.3}$$

where the overlap matrix is

$$Z_{i,n} = \langle 0|\mathcal{O}_i(t)|n\rangle\,. \tag{1.4}$$

In a typical application $C(t)$ is known and we want to determine the energies E_n. We start by truncating the infinite sum in Eq. (1.2) to a finite sum for $n \in [1, N]$ and introduce at least N linearly independent interpolating operators $\mathcal{O}_i(t)$. Then we can find the energies by solving the generalized eigenvalue problem

$$C(t)u_n = \lambda_n(t, t_0)C(t_0)u_n\,, \tag{1.5}$$

where u_n is the kth column of the matrix Z, and $\lambda_n(t, t_0)$ is an approximation to the eigenvalue $\exp[-E_n(t-t_0)]$ of the infinite transfer matrix T^{t-t_0}. They are approximations, because truncating the multiexponential sum introduces errors [1, 2]. We discuss the approximation at greater length below.

II. STAGGERED VARIATIONAL METHOD

When the hadronic correlator involves staggered fermions, the multiexponential expansion includes terms that oscillate in time:

$$C_{ij}(t) = \sum_n \langle 0|\mathcal{O}_i(t)|n\rangle s_n(t) e^{-E_n t} \langle n|\mathcal{O}_j^\dagger(0)|0\rangle \,. \tag{2.1}$$

where the t-dependent sign $s_n(t) = 1$ for a nonoscillating state n and $s_n(t) = (-1)^t$ for an oscillating state.

This oscillation is well known for mesons and baryons constructed from single-time-slice interpolating operators consisting of only staggered fermions [3, 4]. The oscillating component corresponds to a state with parity opposite to that of the nonoscillating component. Since the states often come in pairs, they are sometimes called "parity partners". In the case of a meson with definite charge conjugation, the partner also has the opposite charge conjugation quantum number.

We are interested here in the correlator for a meson arising from a source interpolating operator consisting of a Dirac (Wilson or clover) quark and a staggered antiquark. To construct the hadronic correlator, we first convert the staggered propagator $S(x', x)$ to a "naive" propagator [5], using

$$N(x', x) = \Gamma^\dagger(x')\Gamma(x) S(x', x) \,, \tag{2.2}$$

where, in one convention,

$$\Gamma(x) = \gamma^{x_1}\gamma^{x_2}\gamma^{x_3}\gamma^{x_0} \,. \tag{2.3}$$

It is now standard practice to work with improved staggered fermion propagators S so the resulting "naive" propagator N inherits the improvement.

The resulting propagator $N(x', x)$ carries both color and spin indices and so can be treated on the same footing as the propagator for the Dirac quark $W(y', y)$. So, for example, if the source interpolating operator is a local zero-momentum quark-antiquark bilinear with gamma matrix Γ_A, and, similarly, the sink interpolating operator is a local bilinear with gamma matrix Γ_B, then the resulting hadronic correlator with $x' = (t, \mathbf{x}')$ and $x = (0, \mathbf{x})$ is

$$C(t) = \sum_{\mathbf{x}} \mathrm{Tr}[\Gamma_B N(x', x) \Gamma_A^\dagger W(x, x')] \,, \tag{2.4}$$

where the trace is over both spins and colors.

Now consider a corresponding correlator $C'(t)$ with the source and sink gamma matrices replaced with $\Gamma_A\gamma_0\gamma_5$ and $\Gamma_B\gamma_0\gamma_5$, respectively. This replacement preserves the angular momentum, but reverses the parity of the state and its charge conjugation quantum number, if relevant. It is easy to show that

$$C'(t) = C(t)(-)^t \ . \tag{2.5}$$

because

$$\gamma_0\gamma_5 N(x', x) = (-)^{x'_0 - x_0} N(x', x)\gamma_0\gamma_5 \, . \tag{2.6}$$

Thus with meson correlators involving staggered fermions, there is a symmetry relating correlators for channels of opposite C and P quantum numbers. A given state appears in both correlators, in one of them with no oscillation and in the other, with oscillation.

With the single-time-slice Dirac-plus-staggered interpolating operators we have studied, hadronic correlators typically contain both oscillating and nonoscillating contributions as contemplated in Eq. (2.1). From the discussion of the meson case above, we see that oscillating contribution is associated with a partner state of the opposite P and C. Moreover, if an interpolating operator $\mathcal{O}_i$ is constructed from a hermitian bilinear with gamma matrix Γ_A, the operator constructed from $\Gamma_A\gamma_0\gamma_5$ is antihermitian. Thus

$$\langle n|\mathcal{O}_i(0)|0\rangle = -\langle n|\mathcal{O}_i^\dagger(0)|0\rangle \, . \tag{2.7}$$

A consequence is that the parity partner contributions, in addition to oscillating with a factor $(-)^t$ include an overall minus sign from the antihermiticity noted above. Thus, the correlator has the matrix form

$$C(t) = ZT^t g Z^\dagger \, , \tag{2.8}$$

where $T = g \, \mathrm{diag}\, e^{-E_n}$ and $g = \mathrm{diag}\, s_n(1)$, that is, a diagonal matrix with a plus (minus) sign for nonoscillating (oscillating) states.

The generalized eigenvalue problem is the same as before:

$$C(t)u_n = \lambda_n(t, t_0)C(t_0)u_n \, , \tag{2.9}$$

but with oscillating as well as nonoscillating eigenvalues $\lambda_n(t, t_0)$. We modify the ordering convention so the eigenvalues are in decreasing order according to their magnitudes $|\lambda_n(t, t_0)| > |\lambda_{n+1}(t, t_0)|$ for large t and t_0. If there are N linearly independent interpolating

operators and the multiexponential expansion terminates at the the Nth energy, the generalized eigenvalue problem yields $\lambda_n = s_n(t-t_0)e^{-E_n(t-t_0)}$ exactly. Of course, in practice, the multiexponential expansion does not terminate, so the generalized eigenvalues only approximate $s_n(t-t_0)e^{-E_n(t-t_0)}$. The ALPHA Collaboration used perturbation theory to treat the effect of restoring energy levels with $E_n > E_N$ [2]. Their analysis is easily generalized to the present case with oscillating and nonoscillating states. To second order we have

$$\begin{aligned}\lambda_n(t,t_0) \approx\ & s_n(t-t_0)(1-a_n(t_0))e^{-E_n(t-t_0)} \\ & + \sum_{m>n}^{N} b_{m,n}(t_0)s_m(t-t_0)e^{-E_m(t-t_0)} \\ & - \sum_{m<n} b_{m,n}(t_0)s_m(t-t_0)e^{-(2E_n-E_m)(t-t_0)} + \mathcal{O}(e^{-E_{N+1}(t-t_0)})\,.\end{aligned} \tag{2.10}$$

The coefficients a_n and $b_{m,n}$ depend only upon t_0 and overlap factors:

$$\begin{aligned}a_n(t_0) \approx\ & A_{n,n,N+1}s_n(t_0)s_{N+1}(t_0)e^{-(E_{N+1}-E_n)t_0} \\ & - \left[e^{-2(E_{N+1}-E_n)t_0}|A_{n,n,N+1}|^2 + \sum_{m>n}^{N} b_{n,m,N+1}(t_0)\right]\end{aligned} \tag{2.11}$$

$$b_{m,n}(t_0) \approx |A_{m,n,N+1}|^2 s_n(t_0)s_m(t_0)e^{-(2E_{N+1}-E_n-E_m)t_0}\,, \tag{2.12}$$

where $A_{m,n,N+1}$ is given by the product of overlaps

$$A_{m,n,N+1} = \left(\sum_{i=1}^{N} u^*_{m,i}Z_{i,N+1}\right)\left(\sum_{i=1}^{N} Z^*_{i,N+1}u_{n,i}\right)\,. \tag{2.13}$$

As the number N of linearly independent interpolating operators is increased at fixed t, t_0, m, and n, the factors $e^{-(E_{N+1}-E_n)t_0}$ decrease exponentially, so the coefficients a_n and $b_{m,n}$ vanish exponentially. So, as expected,

$$\lambda_n(t,t_0) \to s_n(t-t_0)e^{-E_n(t-t_0)}\,. \tag{2.14}$$

Alternatively, if t_0 is large for fixed N, m, and n, the exponential factors also suppress the coefficients a_n and $b_{m,n}$ with the same result. In Ref. [2] the ALPHA collaboration argued that to assure a plateau in the "effective energy", *i.e.*, to obtain a good approximation to the above asymptotic form, one should require $t_0 > t - t_0 \gg 0$. However, making N large increases the cost of the calculation, and it is not always possible to make t_0 large and still have a good signal for the hadron correlator. For this reason the Hadron Spectrum

Collaboration, in a more conventional application without staggered fermions, proposed fitting eigenvalues to the form

$$\lambda_n(t,t_0) \approx (1-a_n)e^{-E_n(t-t_0)} + a_n e^{-\bar{E}_n(t-t_0)}\,, \tag{2.15}$$

where the second term approximates higher corrections [6]. With staggered fermions, we simply include terms that oscillate in t, as, for example with the model

$$\begin{aligned}\lambda_n(t,t_0) \approx [1-a_n(t_0)]s_n(t-t_0)e^{-E_n(t-t_0)} + b_n(t_0)s_n(t-t_0)e^{-\bar{E}_n(t-t_0)} + \\ + c_n(t_0)s'_n(t-t_0)e^{-E'_n(t-t_0)} + d_n(t_0)s'_n(t-t_0)e^{-\bar{E}'_n(t-t_0)}\,,\end{aligned} \tag{2.16}$$

where $s'_n(t)$ oscillates if $s_n(t)$ does not, and vice versa. We arrange so that the principal term, *i.e.*, the term with the largest amplitude, is the one with coefficient $1-a_n(t_0)$. Having both oscillating and nonoscillating components is almost never an obstacle to extracting energies. Because the two contributions are functionally very different, there is little chance for confusion. Because $\lambda_n(t_0,t_0)=1$, it is useful to consider imposing the sum rule

$$\Sigma_n \equiv 1 - a_n(t_0) + b_n(t_0) + c_n(t_0) + d_n(t_0) \approx 1\,. \tag{2.17}$$

From Eq. (2.11) we see that the parity partner energies E'_n might not always be equal to the energy of a state, since we may have either $E'_n = E_m$ or $E'_n = 2E_n - E_m$, where E_m is the energy of a nearby state. In principle the same choices apply to the excited state values $\bar{E}_n$ and $\bar{E}'_n$, but in practice these energies could represent a weighted average of an array of possible states including the lowest excluded state E_{N+1}.

If the set of interpolating operators $\mathcal{O}_i$ is sufficiently complete, we expect to be able to separate the oscillating and nonoscillating eigenvalues, meaning that the coefficients of the parity-partner terms should be negligible. This implies that the linear combination of operators

$$\bar{\mathcal{O}}_n = \sum_i \mathcal{O}_i Z^{-1}_{i,k}\,, \tag{2.18}$$

to a good approximation, generates a hadron correlator without an oscillating component. However, it often happens that the set of operators are nearly linearly dependent. For example, if the interpolating operators differ only in a smearing width, we have found that the coefficients $1-a_n$ and c_n can be comparable in magnitude. In that case the eigenvalues contain a significant pair of parity partners, and adding a new interpolating operator to the set might serve, instead, to isolate an excited state, rather than a low-lying parity partner.

III. D_s MESON SPECTRUM

We illustrate the method by considering mesons generated by interpolating operators consisting of a clover (Fermilab) charm quark [7] and a staggered strange antiquark. The lightest of these is the D_s meson. Previous studies of this system with variational methods treated both quarks in the clover formalism [8–12].

A. Ensemble parameters

We work with the MILC ensemble with lattice spacing $a = 0.15089(17)$ [13] fm, generated in the presence of $2 + 1 + 1$ flavors of highly improved staggered sea quarks (HISQ), *i.e.*, equal up and down sea quark masses, plus strange and charm sea quarks with all masses approximately equal to their physical values [14]. The lattice dimension is $32^3 \times 48$. We measured the charm-strange meson correlator on 988 gauge configurations separated by six molecular dynamics time units with eight uniformly spaced source times per configuration. The charm-strange mesons were constructed with a clover (Fermilab) charm quark and a strange HISQ with mass equal to the strange sea quark in the ensemble. We also measured the charmonium correlator to set the charm quark mass. It is tuned so that the splitting between the D_s and η_c rest masses $2M(D_s) - M(\eta_c)$ is approximately equal to its experimental value, as shown in Fig. 1. The resulting hopping parameter is $\kappa_c = 0.1256^{+0.0021}_{-0.0014}$.

To construct the charm-strange meson we consider a variety of single-time-slice, zero-momentum interpolating operators $\mathcal{O}_i$ of the form

$$\mathcal{O}_i(t) = \sum_{\mathbf{x}} \bar{Q}(\mathbf{x}, t) J_i q(\mathbf{x}, t)\,, \tag{3.1}$$

where Q is the clover charm quark field and q is the HISQ field, converted by standard methods to a "naive" Dirac field according to Eq. (2.2). Both fields carry suppressed Dirac spin and color indices. The current operators J_i in this study are listed in Table I. We introduce three types of covariant Gaussian smearing, defined, as usual, in terms of the gauge-covariant Dirac operator $\not{D}$ and a smearing width r_x:

$$S_x = \exp(r_x^2 \not{D}^2/4) \tag{3.2}$$

for $x = a, b, c$ with widths $r_a = 0$ (local operator), $r_b = 1.6$ (only clover quark smeared) and $r_c = \sqrt{2r_b^2} = 2.2$ (both clover and staggered quarks smeared).

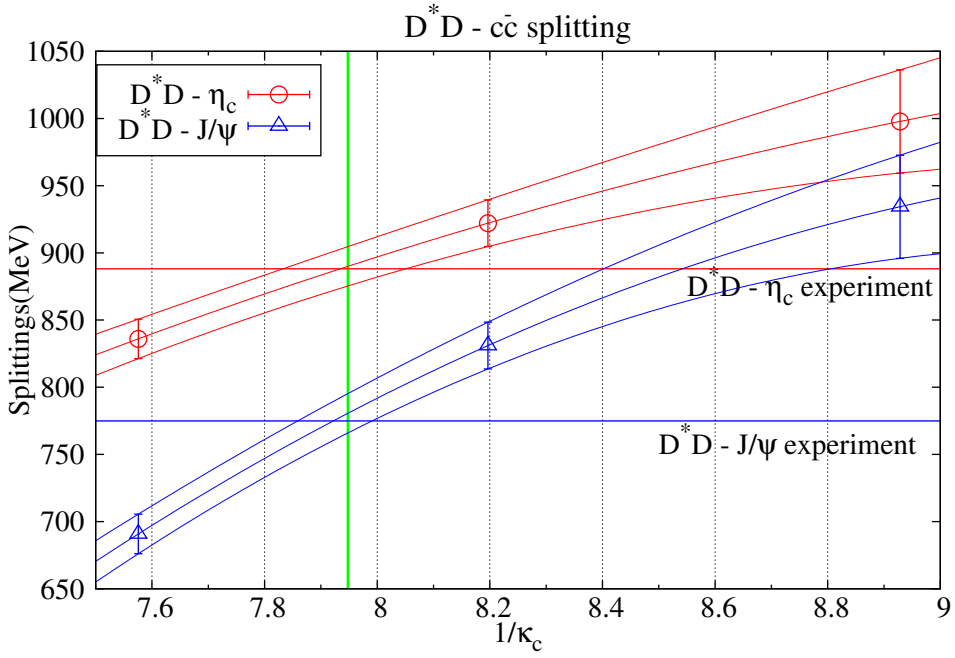

FIG. 1. The rest mass splitting $2M(D_s) - M(\eta_c)$ as a function of $1/\kappa_c$, used for tuning the charm quark mass.

As we have noted, the states belonging to the channels characterized by the opposite-parity irreducible representations (irreps) A_1^+, T_1^+ and T_2^- can be extracted as the parity partners of states in the irreps A_1^-, T_1^- and T_2^+.

B. Effective energies from generalized eigenvalues

Following the procedure described in Sec. II we extract the leading eigenvalues $\lambda_n(t, t_0)$ for each channel. Then, first, we consider the corresponding effective energies. Since each eigenvalue could contain both oscillating (O) and nonoscillating (NO) components, for each eigenvalue we attempt to extract effective energies for both cases:

$$E_{\text{eff}}^{(k)}(t) = \log\left[\lambda^{(k)}(t+1)/\lambda^{(k)}(t)\right] \quad \text{NO} \tag{3.3}$$

$$E_{\text{eff}}^{(k)}(t) = \log\left[-\lambda^{(k)}(t+1)/\lambda^{(k)}(t)\right] \quad \text{O}\,. \tag{3.4}$$

In either case, we find it helpful to smooth the result:

$$\mathcal{E}_{\text{eff}}^{(k)} = \frac{1}{4}\left[E_{\text{eff}}^{(k)}(t+1) - 2E_{\text{eff}}^{(k)}(t) + E_{\text{eff}}^{(k)}(t-1)\right]\,. \tag{3.5}$$

TABLE I. Current operators J_i for constructing interpolating operators $\bar{Q}(\mathbf{x},t)J_i q(\mathbf{x},t)$ for the charm-strange mesons in this study for each of the indicated irreps of the octahedral group (with spatial inversions): O_h. The notation S_x represents a covariant Gaussian smearing operator with one of three smearing widths a, b, c as discussed in the text. The single-time-slice operators typically generate states with both parities. The indicated parity is for the nonoscillating state.

A_1^-	T_1^-	T_2^+
$\gamma_5 \cdot S_{a,c}$	$\gamma_i \cdot S_{a,b,c}$	$\lvert\varepsilon_{ijk}\rvert\, \gamma_j \nabla_k$
$\gamma_t\gamma_5 \cdot S_{a,c}$	$\gamma_t\gamma_i \cdot S_{a,b,c}$	$\lvert\varepsilon_{ijk}\rvert\, \gamma_t\gamma_j \nabla_k$
$\gamma_5\gamma_i \cdot \nabla_i$	$\boldsymbol{I} \cdot \nabla_i$	
$\gamma_t\gamma_5\gamma_i \cdot \nabla_i$	$\gamma_t \cdot \nabla_i$	
	$\varepsilon_{ijk}\gamma_5\gamma_j \nabla_k$	
	$\varepsilon_{ijk}\gamma_t\gamma_5\gamma_j \nabla_k$	

We set the reference time $t_0 = 3$ (4 in the case of T_2^+). In the variational calculation we include all operators in the respective columns of Table I, and we examine results for all six channels $A_1^\pm$, $T_1^\pm$, and $T_2^\pm$. These single-time-slice operators generate states of both parities. The parity indicated in the table is for the nonoscillating state. The resulting effective energies (masses in our zero-momentum case) for both parities are plotted in Fig. 2 as a function of t and tabulated in Table II.

Including all interpolating operators in many cases permits a clean isolation of the parity partners. That is, for a given eigenvalue, often only the oscillating or nonoscillating component is robust, and the partner component is too weak to obtain a statistically significant effective mass. So only the robust states are plotted in Fig. 2 and listed in Table II.

C. Multiexponential fit to generalized eigenvalues

From the foregoing effective mass analysis, we find that when all the interpolating operators in Table I are in use, we effectively isolate the low-lying parity partners. It is interesting to examine the progressive isolation as the dimension N of the interpolating operator basis is increased or as the reference time t_0 is increased. To do this we fit the eigenvalues to

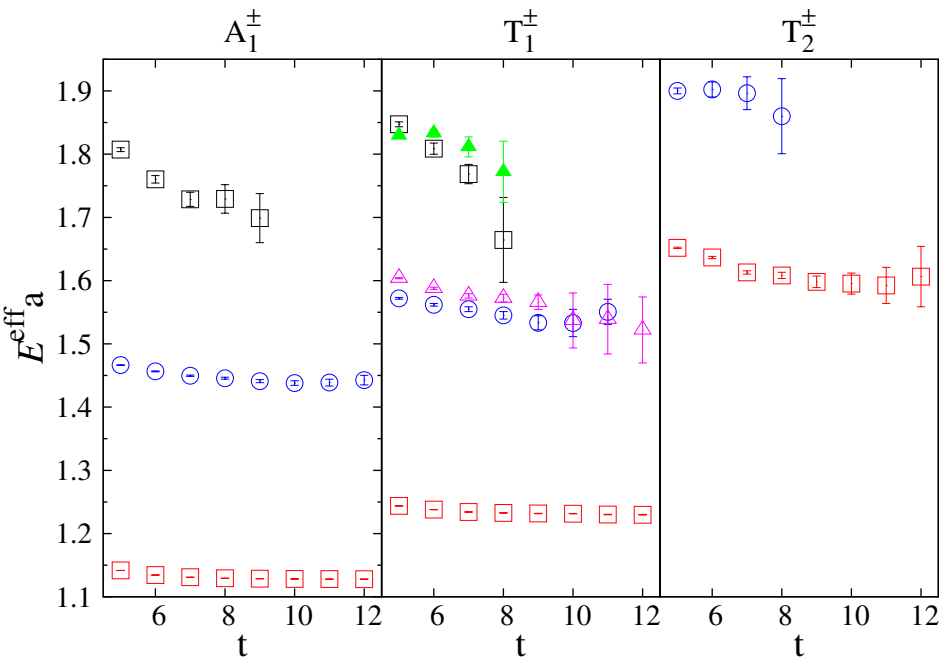

FIG. 2. Smoothed effective masses $\mathcal{E}_{\rm eff}$ from the the eigenvalues in the $A_1^{\pm}$, $T_1^{\pm}$ and $T_2^{\pm}$ charm-strange channels as a function of t. All interpolating operators listed in Table I are used. The reference times are $t_0 = 3$ for $A_1^{\pm}$, $T_1^{\pm}$ and $t_0 = 4$ for $T_2^{\pm}$, which are about 0.45 fm and 0.6 fm, respectively. The plot symbols and level assignments are listed in Table II and discussed in the text.

our preferred model Eq. (2.16), and, for each eigenvalue, we study the effect on the principal amplitude $1 - a_n$ and mass M_n. We discuss results for the $A_1^{\pm}$, $T_1^{\pm}$, and $T_2^{\pm}$ channels separately.

For the fit range we choose $t_{\rm min} = t_0 + 1$ or $t_0 + 2$, and we choose $t_{\rm max}$ to achieve a resonably low χ^2. For most cases, within this fit range, two to four exponentials from our model Eq. (2.16) are enough to get a robust fit result for the chosen low t_0. To impose the constraint Eq. (2.17), we replace one of the amplitude parameters by Σ_n in Eq. (2.17) and constrain Σ_n using a gaussian Bayesian prior with central value and width $(1, \sigma)$. Often the Bayesian constraint is unnecessary.

TABLE II. Classification of states identified from their effective masses shown in Fig. 2. Listed are the eigenvalue indices, whether the principal state is obtained from the oscillating (O) or nonoscillating (NO) effective mass, the plot symbol, the inferred O_h irreducible representation and continuum spin/parity, and the assigned hadronic state [15], if obvious.

n	NO/O	plot symbol	J^P	assignment
		$A_1^\pm$		
0	NO	red squares	A_1^-, 0^-	D_s
1	O	blue circles	A_1^+, 0^+	$D_{s0}^*(2317)$
2	NO	black squares	A_1^-, 0^-	?
		$T_1^\pm$		
0	NO	red squares	T_1^-, 1^-	D_s^*
1	O	blue circles	T_1^+, 1^+	$D_{s1}(2460)$
2	O	purple triangles	T_1^+, 1^+	$D_{s1}(2536)$
3	NO	black squares	T_1^-, 1^-	$D_{s1}^*(2700)$
4	NO	green triangles	T_1^-, 1^-	?
		$T_2^\pm$		
0	NO	red squares	T_2^+, 2^+	$D_{s2}^*(2573)$
1	O	blue circles	T_2^-, 2^-	?

1. $A_1^\pm$ channel

To show how results at fixed t_0 change as the dimension N of the interpolating operator basis is increased, we must choose a sequence of additions to the basis. Obviously, the result depends on how we do that. For the $A_1^\pm$ channel, we start at $N = 2$ with the set $\{\gamma_5 \cdot S_{a,c}\}$ (set A). For $N = 3$ and 4, we include $\{\gamma_t\gamma_5 \cdot S_{a,c}\}$ (set B). Finally for $N = 5$ and 6 we include two operators involving derivatives (set C). Results for the $A_1^\pm$ channel are shown in Fig. 3 and listed in Table III. Note that in Fig. 3, we do not display the result for $n = 2$.

We find, as expected, that as N increases in this way with fixed $t_0 = 3$, the amplitude $1 - a_n$ approaches 1 and the mass M_n stabilizes. At the same time, as shown in the table, the amplitude c_0 of the λ_0 parity partner state decreases from 37% for $N = 2$ to 0.1% for $N = 6$, and the amplitude c_1 of the λ_1 parity partner state decreases from 5% to 0.4%.

For the case $N = 2$, the two $\gamma_5 \cdot S_{a,c}$ interpolating operators couple in almost identical proportions to the lowest nonoscillating and oscillating states. So they are linearly dependent with respect to these two states. The result, as shown in Table III set A, is that both parity partners appear with sizeable amplitudes in the leading eigenvalue λ_0. We also see that adding $\{\gamma_t\gamma_5 \cdot S_{a,c}\}$ (set B) is enough to separate the parity partners with the even parity state now appearing in λ_1. Finally, with the full set of operators, the amplitudes $1 - a_n$ for the partners are greater than 0.8 in their respective eigenvalues. In both cases the state with the next largest amplitude is the "excited" state of the same parity as the leading state.

We note that the higher state $n = 2$ has a substantial "excited" state contribution b_2, possibly because the interpolating operators do not have good overlap with the 2S state, and therefore they couple strongly to other states as well.

Instead of varying N at fixed t_0 we can vary t_0 at fixed N. We find that as t_0 increases with fixed $N = 6$, the amplitude $1 - a_n$ also approaches 1, and the mass M_n stabilizes. We can be slightly more quantitative here. From Eqs. (2.11),(2.11) and (2.12), we see that the coefficient a_n in Eq. (2.16) all tend to decrease exponentially with t_0 at fixed N as

$$e^{-(E_{N+1}-E_n)t_0} A_{n,n,N+1}\,, \tag{3.6}$$

whereas the coefficients b_n, c_n, and d_n decrease exponentially according to

$$e^{-2(E_{N+1}-E_n)t_0} A^2_{n,m,N+1}\,. \tag{3.7}$$

We note that at fixed N, the coefficient $A^2_{n,m,N+1}$ is constant. Indeed, as shown in Fig. 3 panel C, the coefficient $1 - a_n$ can be fit with the exponential form $1 - r_n \exp(-\Delta M_n t_0)$, where r_n and ΔM_n are adjusted to their best fit values.

We also note that the mass values M_0 and M_1 for $t_0 \geq 2$ are statistically consistent, which justifies using low reference times t_0 in conjunction with a multiexponential fit, such as Eq. (2.16), to compensate for unsuppressed contributions from other states. The $t_0 = 6$ value (about 0.9 fm) was obtained from a single exponential fit, because the data were then insufficient to determine excited state contributions.

2. $T_1^{\pm}$ channel

In Fig. 4 and Table V, we show the progressive isolation of low-lying parity partners in the $T_1^{\pm}$ channel. For $N = 2$ we use only $\{\gamma_i \cdot S_{a,c}\}$ (set A). For $N = 3$, 4, 5, and 6, we

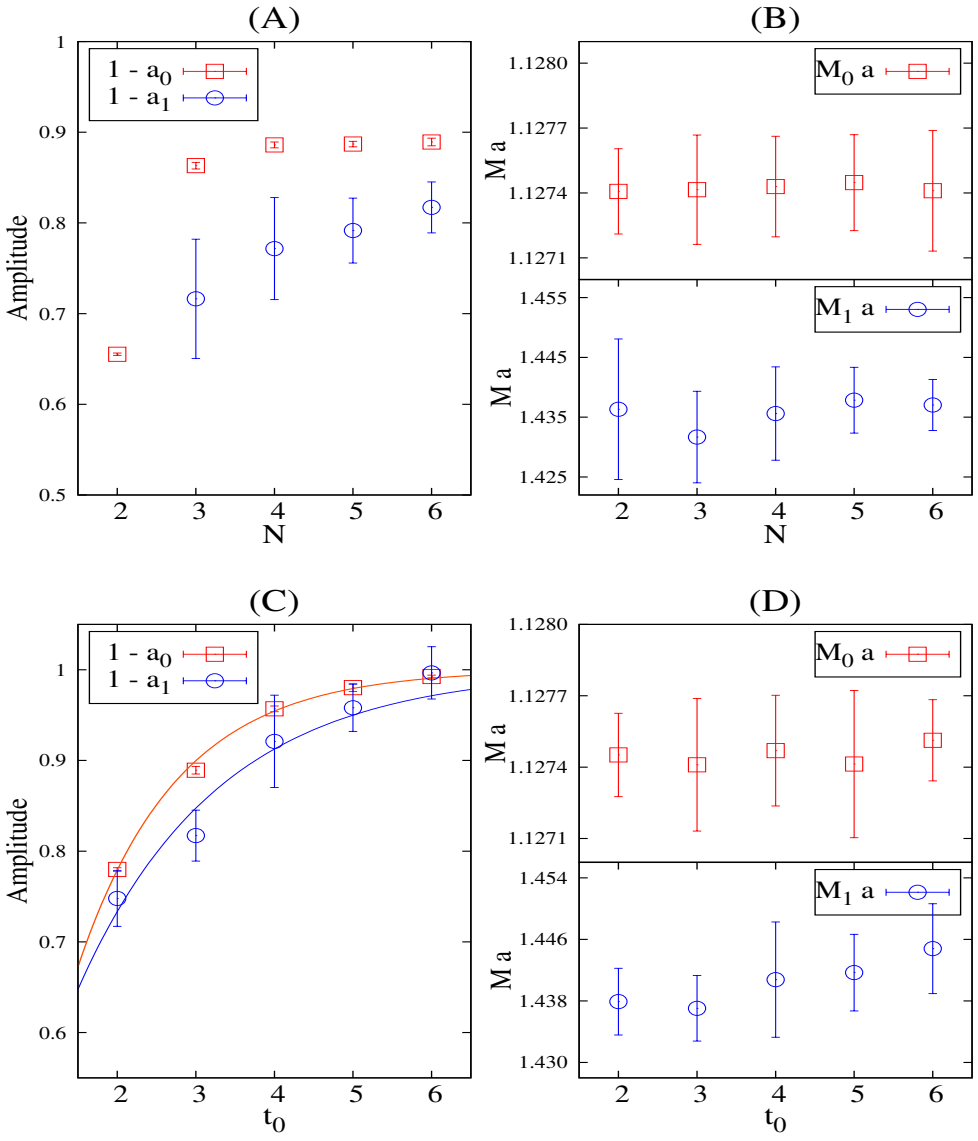

FIG. 3. Progressive improvement in the isolation of parity partner eigenstates with the increasing dimension N of the interpolating operator basis. Improvement is demonstrated for the two leading eigenvalues λ_0 and λ_1 in the $A_1^{\pm}$ channel by examining the principal coefficients and masses from a fit to Eq. (2.16). Panels A and C show the principal fit coefficients $1 - a_0$ and $1 - a_1$ and panels B and D, the masses $M_0 = E_0$ and $M_1 = E_1$ as a function of (A,C) the number of interpoling operators N and (B,D) the reference time t_0. In panels A and B the interpolating operators are added in the order discussed in the text while fixing $t_0 = 3$. In panels C and D t_0 is varied while fixing $N = 6$. We see that in both cases the principal coefficient approaches one, indicating effective isolation of the state. The solid lines represent a fit to the function $1 - r_n e^{-\Delta M_n t_0}$, adjusting both r_n and M_n.

TABLE III. Fit results for the eigenvalues of the $A_1^{\pm}$ channels for three different interpolating operator sets with reference time $t_0 = 3$. The fit parameters a_n, b_n, c_n, d_n, E_n, $\bar{E}_n$, E'_n and $\bar{E}'_n$ are defined in Eq. (2.16). In Set (A), the parity partner state is so strongly mixed that E'_0 and E_1 are almost degenerate. In set (B) and (C), to get the reasonable fit for the ground states, 4-exponential fit is required, which is 3-nonoscillating and 1-oscillating, instead of 2-nonoscillating and 2-oscillating. The third nonoscillating state amplitudes and masses are represented by $\tilde{b}_n$ and $\tilde{E}_n$. The fit information is displayed in Table IV.

set (A): $\{\gamma_5 \cdot S_{a,c}\}$										
n	$1-a_n$	E_n	b_n	$\bar{E}_n$	$\tilde{b}_n$	$\tilde{E}_n$	c_n	E'_n	d_n	$\bar{E}'_n$
0	0.655(1)	1.1274(2)	0.074(6)	1.74(9)	0.5(3)	4.3(7)	−0.165(5)	1.4333(49)	−0.15(14)	2.56(53)
1	0.13(2)	1.436(12)	1.1(2)	3.42(9)	0.33(7)	1.95(11)	−0.017(8)	1.601(79)	−0.5(6)	3.0(7)

set (B): $\{\gamma_5 \cdot S_{a,c}\}$ and $\{\gamma_t\gamma_5 \cdot S_{a,c}\}$								
n	$1-a_n$	E_n	b_n	$\bar{E}_n$	$\tilde{b}_n$	$\tilde{E}_n$	c_n	E'_n
0	0.886(4)	1.1274(3)	0.0142(5)	1.41(28)	0.091(9)	2.04(16)	−0.0047(38)	2.06(32)
1	0.781(25)	1.4369(43)	0.151(2)	1.94(12)	–	–	−0.049(3)	1.781(26)

set (C): all A_1^- operators in Table I								
n	$1-a_n$	E_n	b_n	$\bar{E}_n$	$\tilde{b}_n$	$\tilde{E}_n$	c_n	E'_n
0	0.889(4)	1.1274(3)	0.0144(4)	1.40(26)	0.089(11)	1.99(11)	−0.0010(9)	1.67(30)
1	0.810(31)	1.4361(46)	0.173(3)	1.855(87)	–	–	−0.0039(18)	1.67(17)
2	0.558(51)	1.723(18)	0.441(6)	2.66(28)	–	–	−0.081(19)	2.005(86)

include $\{\gamma_t\gamma_i \cdot S_{a,b,c}\}$ (set B), respectively. Finally, we include the remaining operators in Table I involving derivatives to reach $N = 10$ (set C). Note that in Fig. 4, we do not show the results for $n = 3$ and 4.

As with the $A_1^{\pm}$ case we find that a set of operators that differ only by their degree of smearing (set A) is ineffective in separating the parity partners, so eigenvalue λ_0 contains both of them. However, unlike the $A_1^{\pm}$ channel, the $T_1^{\pm}$ channel has two fairly closely spaced T_1^+ states. So the oscillating term in λ_0 in set A could represent a mixture of both. Adding

TABLE IV. Fit information for the eigenvalues of the $A_1^{\pm}$ channels. Σ_n represents $1 - a_n + b_n + c_n + d_n$. The next column shows its prior central value and width. We found that it is close to 1, as expected from the sum rule of Eq. (2.17), as long as N is large enough.

	n	NO/O	Σ_n	prior $\pm$ width	fit type	fit range	χ^2/d.o.f
set (A)	0	NO	1.00(2)	1 ± 0.02	5-exp	4-16	2.0/3
	1	O	1.00(2)	1 ± 0.02	5-exp	4-16	2.4/3
set (B)	0	NO	0.986(4)	1 ± 0.2	4-exp	4-20	5.6/9
	1	O	0.883(6)	1 ± 0.2	3-exp	4-18	6.8/9
set (C)	0	NO	0.992(3)	1 ± 0.1	4-exp	4-20	5.5/9
	1	O	0.978(5)	1 ± 0.1	3-exp	4-18	7.3/9
	2	NO	0.944(87)	1 ± 0.1	3-exp	4-11	3.3/2

the $\{\gamma_t\gamma_i \cdot S_{a,b,c}\}$ operators helps partly in separating the states, but λ_0 for that set still has a strong oscillating component. A nearly complete separation occurs only after nine or more operators are included (set C). Then λ_0 contains only the nonoscillating state and the two oscillating states appear separately in λ_1 and λ_2.

We also see that for higher excitations, the separation of states is less clean. Level $n = 3$ requires a substantial amplitue b_3, and level 4 requires a substantial opposite-parity amplitude c_4.

Panels C and D in Fig. 4 show the principal-state amplitudes and masses from fits as a function of the reference time, t_0. Since $N = 10$ is fixed, $A_{n,n,N+1}$ is constant, and the amplitude a_0 should decrease exponentially according to Eq. (3.6). When $t_0 = 5$, the opposite parity contributions become negligible, and the mass can be extracted to good approximation with a single-exponential fit. Even so, as shown in panel D, all masses are statistically equivalent over the whole range of t_0 displayed. This equivalence suggests that one can extract the desired mass for low t_0 using a multi-exponential fit with three or four exponentials, as in Eq. (2.1).

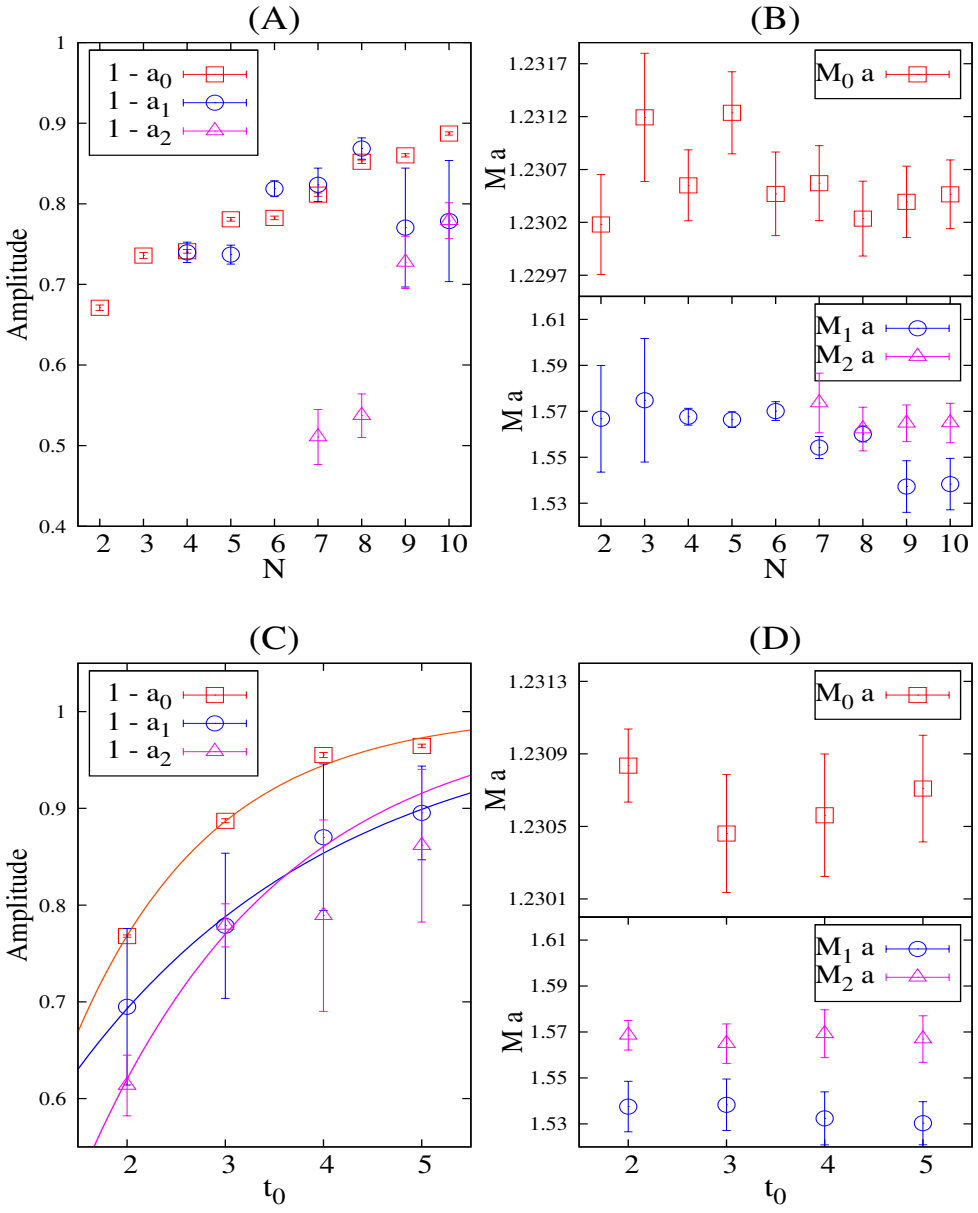

FIG. 4. As in Fig. 3, but for the lowest two states in the $T_1^{\pm}$ channels. The operator sets are defined in the text.

3. $T_2^{\pm}$ channel

Finally, Table VII lists fit results for the $T_2^{\pm}$ channel. Because there are only a few interpolating operators, the parity partners are not well separated at $t_0 = 4$. Thus even at reasonably low t_0, the multiexponential fit again helps to compensate for contamination from other unsuppressed exponential contributions.

TABLE V. Fit results for the eigenvalues of the $T_1^{\pm}$ channels for three different interpolating operator sets with reference time $t_0 = 3$. The notation is the same as in Table III.

set (A): $\{\gamma_5 \cdot S_{a,c}\}$										
n	$1-a_n$	E_n	b_n	$\bar{E}_n$	$\tilde{b}_n$	$\tilde{E}_n$	c_n	E'_n	d_n	$\bar{E}'_n$
0	0.671(3)	1.2302(5)	0.071(1)	1.76(13)	0.6(3)	3.83(29)	−0.142(6)	1.523(7)	−0.2(3)	2.85(77)
1	0.051(9)	1.567(23)	0.41(4)	2.31(13)	1.0(3)	4.9(1.7)	−0.06(2)	1.69(5)	−0.4(1)	2.4(2)

set (B): $\{\gamma_i \cdot S_{a,b,c}\}$ and $\{\gamma_t\gamma_i \cdot S_{a,b,c}\}$								
n	$1-a_n$	E_n	b_n	$\bar{E}_n$	c_n	E'_n	d_n	$\bar{E}'_n$
0	0.784(2)	1.2306(4)	0.164(3)	2.179(99)	−0.073(2)	1.5382(76)	–	–
1	0.798(33)	1.5647(92)	0.286(2)	2.94(87)	−0.081(20)	1.667(71)	–	–
2	0.276(49)	1.669(49)	0.819(1)	2.44(14)	−0.097(10)	1.648(30)	–	–

set (C): all T_1^- operators listed in Table I								
n	$1-a_n$	E_n	b_n	$\bar{E}_n$	c_n	E'_n	d_n	$\bar{E}'_n$
0	0.872(2)	1.2305(3)	0.0856(3)	1.879(35)	−0.0108(8)	1.586(28)	–	–
1	0.774(80)	1.538(12)	0.187(6)	1.94(19)	−0.012(3)	1.59(10)	–	–
2	0.761(47)	1.569(10)	0.256(17)	2.44(66)	−0.0020(29)	1.27(25)	−0.06(19)	2.6(1.8)
3	0.529(90)	1.739(31)	0.482(4)	2.34(12)	−0.017(3)	1.556(68)	–	–
4	0.720(23)	1.8248(89)	0.504(3)	4.11(55)	−0.22(5)	2.323(91)	–	–

D. Comparison with observed states

Even though we are working at only one lattice spacing with quark masses close, but not finely tuned, to their physical values, and we have not considered effects of two-meson channels, it is tempting to compare our results with the experimentally known masses[15]. This is done in Fig. 5 and Table IX, including tentative assignments.

TABLE VI. Fit information for the eigenvalues of the $T_1^{\pm}$ channels. The notation is the same as in Table IV.

	n	NO/O	Σ_n	prior $\pm$ width	fit type	fit range	χ^2/d.o.f
set (A)	0	NO	1.00(5)	1 ± 0.05	5-exp	4-17	5.9/4
	1	O	1.00(5)	1 ± 0.05	5-exp	4-17	3.5/4
set (B)	0	NO	0.87(3)	1 ± 0.3	3-exp	5-19	6.5/9
	1	O	1.00(30)	1 ± 0.3	3-exp	5-17	5.9/7
	2	NO	0.97(9)	1 ± 0.1	3-exp	5-11	0.4/1
set (C)	0	NO	0.962(2)	1 ± 0.1	3-exp	4-20	11.2/11
	1	O	0.952(11)	1 ± 0.1	3-exp	4-17	5.2/8
	2	O	0.948(58)	1 ± 0.1	4-exp	4-13	0.9/2
	3	NO	0.994(19)	1 ± 0.02	3-exp	4-10	2.2/1
	4	NO	0.991(99)	1 ± 0.1	3-exp	4-11	1.3/2

TABLE VII. Fit results for the eigenvalues of the $T_2^{\pm}$ channels with reference time $t_0 = 4$. The notation is the same as in Table III.

set (C): all T_2^+ operators listed in Table I								
n	$1 - a_n$	E_n	b_n	$\bar{E}_n$	c_n	E'_n	d_n	$\bar{E}'_n$
0	1.01(11)	1.594(16)	0.338(6)	2.17(27)	−0.34(15)	1.890(18)	–	–
1	1.34(3)	1.903(12)	–	–	−0.35(4)	2.11(7)	–	–

TABLE VIII. Fit information for the eigenvalues of the $T_2^{\pm}$ channels. The notation is the same as in Table IV.

	n	NO/O	Σ_n	prior $\pm$ width	fit type	fit range	χ^2/d.o.f
set (A)	0	NO	1.009(60)	1 ± 0.08	3-exp	5-15	4.1/5
	1	O	0.99(1)	–	2-exp	5-13	4.5/5

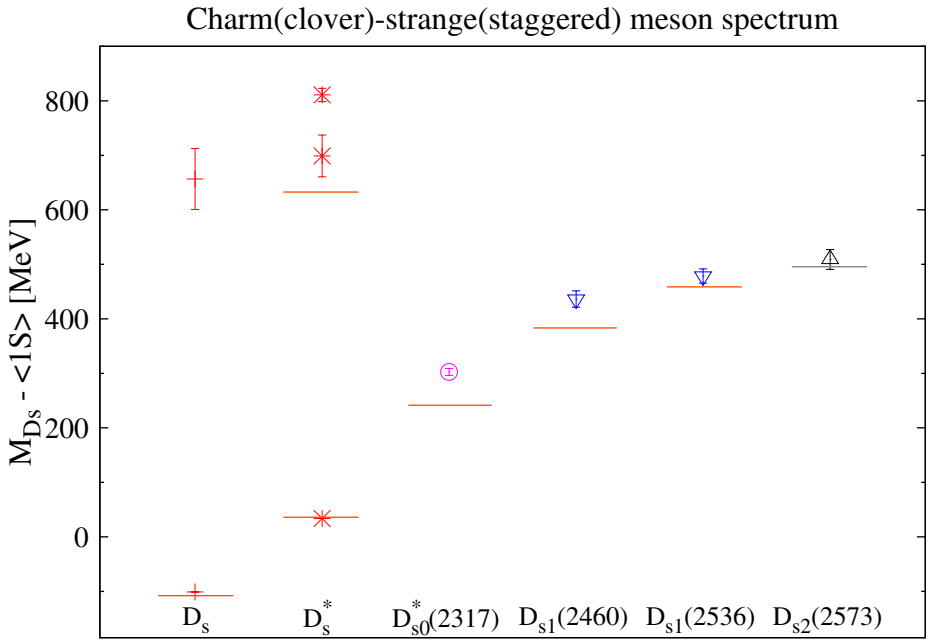

FIG. 5. Comparison of our crude theoretical charm-antistrange meson spectrum (symbols with errors) with experimental values (short horizontal lines) with tentative assignments of the levels. Mass splittings are shown relative to the spin-averaged D_s $1S$ state, namely $\overline{1S} = \frac{1}{4}(D_s + 3D_s^*)$.

TABLE IX. Mass splittings in the D_s spectrum. The experimental splittings are calculated relative to the spin-averaged D_s $1S$ state, based on values in Ref. [15].

	Experiment [MeV]	Lattice [MeV]
$D_s^* - D_s$	143.8 ± 0.4	134.77 ± 0.51
$D_s - \overline{1S}$	-107.9 ± 0.5	-101.08 ± 0.38
$D_s^* - \overline{1S}$	35.9 ± 0.6	33.69 ± 0.13
$D_{s1}^*(2700) - \overline{1S}$	632.7 ± 4	698.9 ± 38.4
$D_{s0}(2317) - \overline{1S}$	241.5 ± 0.7	302.6 ± 6.3
$D_{s1}(2460) - \overline{1S}$	383.3 ± 0.7	436.2 ± 15.0
$D_{s1}(2536) - \overline{1S}$	458.8 ± 0.4	478.5 ± 13.1
$D_{s2}(2573) - \overline{1S}$	496.3 ± 1.0	508.9 ± 18.3

IV. CONCLUSION

The variational method is widely used to determine the hadronic spectrum in lattice QCD. With this method the variational basis is constructed by acting on the vacuum with a linear combination of a variety of interpolating operators of appropriate conserved quantum numbers. The eigenvalues of a resulting generalized eigenvalue problem then determine the spectrum. We described an extension of the method to single-time-slice interpolating operators involving staggered fermions where the effective transfer matrix has both negative and positive eigenvalues.

We presented a straightforward generalization of the perturbative treatment of the ALPHA Collaboration [2] that provides an estimate of the error in the variational eigenvalue estimates resulting from the truncation to a finite interpolating operator basis. Motivated by the perturbative treatment, we presented a simple multiexponential expansion of the eigenvalues for a more accurate determination of the energy levels. The multiexponential approach allows one to relax, to some extent, impractical constraints that require large reference times in the generalized eigenvalue problem.

We illustrated the method with a lattice QCD study of the orbital and radial excitations of the D_s meson. In this calculation, the charm quark was modeled in the clover fermion formulation (Fermilab interpretation) and the strange quark, in the highly improved staggered quark (HISQ) formulation. All quarks, including sea quarks, had approximately physical masses. We found that with a sufficiently large and diverse basis, the variational method is capable of separating low-lying parity-partner states, placing them in separate eigenvalues of the transfer matrix. We showed that large reference times lead to the suppression of extraneous multiexponential contributions, as expected. Finally, we compared our results for the excitations with the experimental values and found satisfactory agreement, considering the coarseness of the lattice and the omission of multihadron interpolating operators.

ACKNOWLEDGEMENT

We thank Daniel Mohler and Heechang Na for useful discussions. This work was supported by the U.S. National Science Foundation under grant NSF PHY10-034278 and the U.S. Department of Energy under grant DE-FC02-12ER41879. Computations were car-

ried out on the LQCD clusters at Fermilab and at the Utah Center for High Performance Computing.

---

[1] M. Luscher and U. Wolff, Nucl.Phys. **B339**, 222 (1990).

[2] B. Blossier, M. Della Morte, G. von Hippel, T. Mendes, and R. Sommer, JHEP **0904**, 094 (2009), arXiv:0902.1265 [hep-lat].

[3] M. F. Golterman, Nucl.Phys. **B278**, 417 (1986).

[4] M. F. Golterman and J. Smit, Nucl.Phys. **B255**, 328 (1985).

[5] M. Wingate, J. Shigemitsu, C. T. Davies, G. P. Lepage, and H. D. Trottier, Phys.Rev. **D67**, 054505 (2003), arXiv:hep-lat/0211014 [hep-lat].

[6] L. Liu *et al.* (Hadron Spectrum Collaboration), JHEP **1207**, 126 (2012), arXiv:1204.5425 [hep-ph].

[7] A. X. El-Khadra, A. S. Kronfeld, and P. B. Mackenzie, Phys.Rev. **D55**, 3933 (1997), arXiv:hep-lat/9604004 [hep-lat].

[8] D. Mohler and R. M. Woloshyn, Phys.Rev. **D84**, 054505 (2011), arXiv:1103.5506 [hep-lat].

[9] G. Bali, S. Collins, S. Durr, Z. Fodor, R. Horsley, C. Hoelbling, S. D. Katz, I. Kanamori, S. Krieg, T. Kurth, L. Lellouch, T. Lippert, C. McNeile, Y. Nakamura, D. Pleiter, P. Perez-Rubio, P. Rakowh, A. Schafer, G. Schierholz, K. K. Szabo, F. Winter, and J. Zanotti, PoS LATTICE2011 (2011), hep-lat:1108.6147 [arXiv].

[10] G. Bali, S. Collins, and P. Perez-Rubio, J.Phys.Conf.Ser. **426**, 012017 (2013), arXiv:1212.0565 [hep-lat].

[11] G. Moir, M. Peardon, S. M. Ryan, C. E. Thomas, and L. Liu, JHEP **05**, 021 (2013), arXiv:1301.7670 [hep-ph].

[12] D. Mohler, C. B. Lang, L. Leskovec, S. Prelovsek, and R. M. Woloshyn, Phys.Rev.Lett. **111**, 222001 (2013), arXiv:1308.3175v3 [hep-lat].

[13] A. Bazavov *et al.* (Fermilab Lattice, MILC), Phys.Rev. **D90**, 074509 (2014), arXiv:1407.3772 [hep-lat].

[14] A. Bazavov *et al.* (MILC Collaboration), Phys.Rev. **D87**, 054505 (2013), arXiv:1212.4768 [hep-lat].

[15] K. Olive *et al.* (Particle Data Group), Chin.Phys. **C38**, 090001 (2014).